Non-iterative moment capacities of complex composite beams using Fourier series

Int J Adv Struct Eng (2017) 9:37–49
DOI 10.1007/s40091-016-0147-4

ORIGINAL RESEARCH

Non-iterative moment capacities of complex composite beams using Fourier series

Airil Y. Mohd Yassin[1] · **David A. Nethercot**[2]

Received: 6 May 2016 / Accepted: 2 December 2016 / Published online: 28 December 2016

Abstract A generic procedure is formulated for the determination of the moment capacity of composite beams having a complex cross-section. The key feature is the use of Fourier series to convert the piecewise functions of the cross-sectional stress distribution into a single-rule function. This eliminates the need for several capacity expressions to cover different stress stages, since the procedure permits the use of the general moment capacity expression. It also eliminates any iteration process when determining the location of the neutral axis since equilibrium of the cross-section can be satisfied explicitly. Numerical examples are given to demonstrate the validation and the applications of the formulation.

Keywords Moment capacity · Stress distribution · Fourier's series · Composite beam · Cold-formed steel

Introduction

Since a composite beam is primarily a flexural member, the most important design requirement is usually the provision of adequate moment capacity. This is calculated as the internal moment produced by the flexural stresses during the bending of the beam. The degree of difficulty in determining the moment capacity increases as the beam becomes more complex; this can be due to the geometry, the material properties or a combination of the two. Furthermore, the difficulty is magnified by the various possible stress states of a composite beam's cross-section as indicated in Fig. 1.

These stress states are associated with different premature modes of failure. In the design of a composite beam, some of the possible premature forms of failure are listed below:

1. Local buckling
   - Local buckling occurs due to the bending compressive stress. Early occurrence of the phenomenon limits the stress development in the cross-section (Wright 1993, 1995; Uy and Bradford 1994, 1995a, 1996).
2. Crushing of concrete
   - In contemporary composite beams, i.e., profiled composite beams (Oehlers et al. 1994; Uy and Bradford 1995b) PCFC beams (Mohd Yassin and Nethercot 2007), there is a trend to provide concrete elements throughout the depth of the beam. Such a configuration introduces the possibility for the concrete to crush prior to the full yielding of the steel section, thus leaving the latter in an elastoplastic condition.
3. Fracture and debonding of shear connection
   - Although fracture of shear connection and debonding is unlikely to occur, allowance for such considerations may be necessary (Teng et al. 2001; Oehlers et al. 1994).
4. Fracture of strengthening elements
   - For certain forms of reinforcement an allowance for the fracture of the strengthening elements, i.e.,

✉ Airil Y. Mohd Yassin
airil.yasreen@utp.edu.my

[1] Civil and Environmental Engineering Department, Universiti Teknologi PETRONAS, 32610 Seri Iskandar, Perak, Malaysia

[2] Civil and Environmental Engineering Department, Imperial College London, London SW7 2AZ, UK

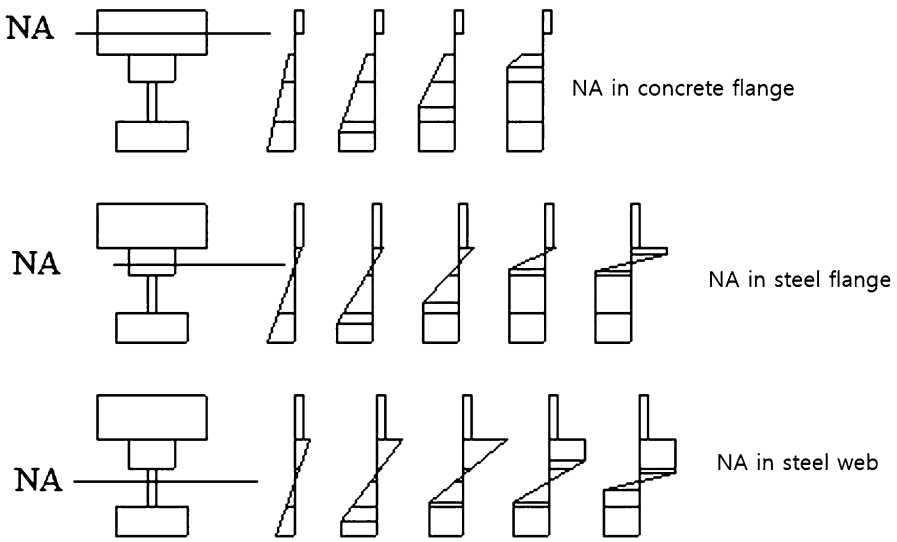

Fig. 1 Possible stress states

FRP, GFRP may be necessary (Oehlers et al. 1994).

All the complexities mentioned above make the determination of the moment capacity of a complex composite beam a task best handled by a computer program. In developing a generic computer program, it is better to use general mathematical expressions able to cover a wide range of possibilities with minimal end-user intervention. In the determination of the moment capacity of a beam, the use of general expressions requires that the stress distribution can be expressed as a single-rule function—this is the focus of this paper.

Review of existing method of analyses

Previous studies of composite beams can be grouped into two classes: cross-sectional analysis and global analysis. Whilst the former concern only the critical cross-sections along the beam span, the latter treats the beam as a whole. Consequently, cross-sectional analysis is simpler to conduct. Despite the differences, all the existing methods employ iterative approaches when determining the location of the neutral axis, resulting in the need for iterative processes when calculating the moment capacity of the composite beam. The general steps may be stated as:

- Step 1: divide the cross-section into strips (or fibers)
- Step 2: assume a location for the NA
- Step 3: calculate the compressive and the tensile resultants and obtain the residual between these resultants
- Step 4: assess whether the residual is less than the specified tolerance, if so the analysis can proceed to the next stage, else, repeat the steps again until convergence is obtained

Cross-sectional analysis

Lodygowski and Szumigala (1992) divided an encased steel beam into strips, where the stress resultants were computed and balanced throughout the cross-section. The procedure for determination of the location of the plastic neutral axis was the same as that listed above, but the convergence algorithm was not detailed in the paper. Similar to Lodygowski and Szumigala, Uy and Bradford (1995b) subdivided a profiled composite beam into horizontal ‘slices’. However, they provided a more detailed description for the iteration and the convergence processes. The location of the NA is increased by a fraction of the beam’s depth until the total of the resultants changes sign, marking the attainment of the larger compressive resultants as compared to the tensile resultants. Then, the method of bisections is used to converge on the value of the location of the NA for which the total of resultants approaches zero to a given accuracy. Oehlers et al. (1994) described a procedure for the determination of the flexural capacities of RC beams stiffened with plates or FRP that is conceptually applicable to any beam. The procedure is based on the known value of failure strains and, for this type of beam, the failure strains can either be concrete crushing strain, debonding strain of the stiffening materials or the plate fracture strain. Mohd Yassin and Nethercot (2007) proposed a procedure to determine the cross-sectional properties of composite beams having complex cross-sections. The key feature is the use of functions to describe the shape of the cross-section. The motivation came from the development of a new type of composite beam, termed a

pre-cast cold-formed composite beam or PCFC beam. In the procedure, the iterative process for the determination of the location of the NA is expressed systematically to suit computer programming. But this procedure is still discrete in nature. Furthermore, as compared to the aforementioned works, this procedure is not appropriate for all stress stages since it is based on the rectangular stress block assumption. However, the procedure provides general computer programming guidelines to cater for general cross-sections while the aforementioned works are best suited to rectangular cross-sections.

Global analysis

Global analysis of composite beams deals with the derivation and the solution of the differential equations governing the behavior of the composite beams. It was first carried out by Newmark et al. (1951) and closed-form solutions are available for simplified elastic considerations (Robinson and Naraine 1998; Roberts and Haji-Kazemi 1989; Taljsten 1997; Smith and Teng 2001). Allowance for differences in the curvature posed difficulty even for the elastic case. In solving such a problem, Adekola (1968) employed the finite difference method (FDM) when solving the coupled differential equations in terms of the normal and the interface shear stresses. For nonlinear problems, finite element methods (FEM) would be the best way to proceed. Displacement-based, force-based and mixed formulations of finite element methods have been derived and updated covering linear and nonlinear problems (Ayoub and Filippou 2000; Dall'Asta and Zona 2002). A comparative study in terms of adequacy and rigor between FEM, direct stiffness method and FDM in analyzing composite beam problems has recently been carried out by Ranzi et al. (2006).

Despite the rigorous nature of FEM, there is a need to balance accuracy and practicality. The work by Sousa and Muniz (2007) is an example of this kind. The idea is that whilst the overall analysis employs FEM, it is simplified at cross-sectional level by the consistent stress approach. In other words, continuum mechanics and strength of materials approaches are employed at global and cross-sectional levels, respectively. But, since the stress–strain curve was represented by a piecewise cubic expression, the work still discretized the cross-section according to the stress state. Due to the piecewise nature, it was necessary to determine, for each material, the regions over which each individual polynomial expression is valid. This again led to an iterative process. Nevertheless, its extension to accommodate the finite element formulation makes this superior to the rest of the cross-sectional analyses described in "Cross-sectional analysis".

Summary of review

Based on the foregoing review of the existing approaches to cross-sectional and global analyses, it is clear that the extent of difficulty in the calculation procedures depends on;

1. Number of materials in the cross-section
2. Complexity of the shape of the cross-section
3. Complexity of the material stress–strain relationship
4. Number of possible premature failure modes.

Also, it can be concluded that the existing iterative approaches are best for rectangular (or regular) shapes and a bilinear stress–strain curve. Therefore, a non-iterative procedure able to cater for irregular cross-sections and non-linear flexural stress distributions is very much needed. This is achieved herein with the use of Fourier series, (termed hereafter as FS) to represent the piecewise functions of the known stress distribution as a single-rule function.

Fourier series (FS)

It is well known that FS are able to approximate a set of piecewise functions as a single-rule function; the accuracy depends on the number of terms and satisfaction of Dirichlet's theorem. Since the stress distribution over the cross-section is a set of piecewise functions, then FS should be suitable for the present application.

For ease of understanding, some relevant derivations of Fourier series are provided. Firstly, FS will be derived to represent the stress–strain curve of the material as a single-rule function. This is followed by the derivation of an FS flexural stress distribution for a single material member. Finally, an FS flexural distribution for a composite beam member is given.

Stress–strain FS formulation

The best way to describe the FS formulation to represent the stress–strain curve of a material as a single-rule function is by direct demonstration. Herein, the formulation for a bilinear steel material model with hardening is demonstrated.

Figure 2 shows the hardening model that is usually assumed for high-strength steel. The model comprises two linear functions. For high-strength steel, since the yield point is not obvious, the yielding strain ε_y is usually taken as 0.2% corresponding to the proof stress. The hardening part of the model is defined by the reduced modulus, γE_s where γ is a reduction factor. The piecewise functions of the model can be given as:

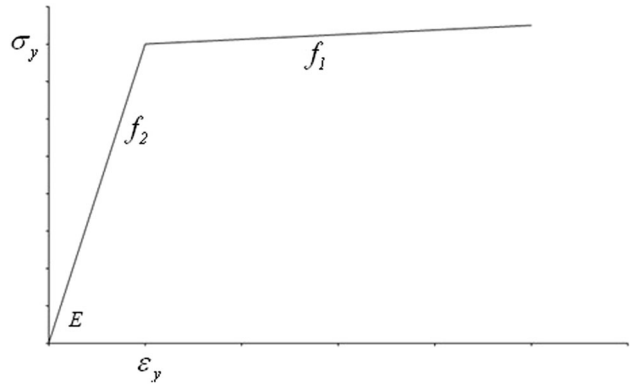

Fig. 2 Steel material model with hardening

$$\sigma = \begin{cases} f_1 = \gamma E\varepsilon + \sigma_y & \text{if} \quad \varepsilon_y \le \varepsilon \\ f_2 = E\varepsilon & \text{if} \quad 0 \le \varepsilon \le \varepsilon_y \\ f_3 = f_2 & \text{if} \quad -\varepsilon_y \le \varepsilon \le 0 \\ f_4 = \gamma E\varepsilon - \sigma_y & \text{if} \quad \varepsilon \le -\varepsilon_y, \end{cases} \tag{1}$$

where σ_y is the intersection of f_1 at the stress axis.

Based on Eq. (1), the Fourier coefficient of the nth term, a_n, can be obtained as:

$$a_n = \frac{2}{\varepsilon_L}\left[\int_{\varepsilon_y} f_1 \sin\left(\frac{n\pi\varepsilon}{\varepsilon_L}\right)d\varepsilon + \int_0^{\varepsilon_y} f_2 \sin\left(\frac{n\pi\varepsilon}{\varepsilon_L}\right)d\varepsilon + \int_{-\varepsilon_y}^{0} f_3 \sin\left(\frac{n\pi\varepsilon}{\varepsilon_L}\right)d\varepsilon + \int^{-\varepsilon_y} f_4 \sin\left(\frac{n\pi\varepsilon}{\varepsilon_L}\right)d\varepsilon\right]. \tag{2}$$

Once a_n is determined, the FS for the stress–strain curve can be given as:

$$\sigma_{FS} = \sum_1^n b_n \sin\left(\frac{n\pi\varepsilon}{\varepsilon_L}\right). \tag{3}$$

Figure 3 shows the FS representation of a typical stress–strain curve with hardening for various numbers of terms.

For concrete, the compressive and the tension behavior can be modeled together. The preceding procedure applies to such a modeling. A typical stress–strain curve for concrete based on Carreira and Chu (1985) for the compressive part is shown in Fig. 4.

FS formulation for cross-sectional flexural stress distribution

Preceding discussion demonstrates the FS representation of the material stress–strain curve. Since the main interest is determination of the moment capacity of beams, the procedure needs to be extended at cross-sectional level. A general stress distribution acting on a beam cross-section is shown in Fig. 5. The piecewise function of the distribution is given as:

$$\sigma(y) = \begin{cases} \cdot \\ \cdot \\ f_i \quad \text{if} \quad dep + y_i \le y \le dep + y_{i-1}, \\ \cdot \\ \cdot \end{cases} \tag{4}$$

where $i = 1\ldots j$, and j is the total number of functions. The integration limits y_i measured from the NA are given as:

$$y_i = \frac{\varepsilon_i}{\varepsilon_L} y_L, \tag{5}$$

where ε_L and y_L are the limiting strain (or the known strain) and its location, respectively; the latter is measured from the NA. All the terms in Eq. (5) are direction sensitive, with those above *dep* taken as positive and vice versa. With these definitions in place, the Fourier coefficients b_n can be given in terms of *dep* as:

$$b_n = \frac{2}{L}\left[\cdots + \int_{dep+y_{i-1}}^{dep+y_i} f_i \sin\left(\frac{n\pi y}{L}\right)dy + \cdots\right], \tag{6}$$

where L is the FS range or period and n is the nth term of the series. L is the span which extends beyond the depth of the cross-section, D as shown in Fig. 6.

However, the value of L cannot be determined a priori exactly because it depends on the location of the NA and thus the value of, *dep*. But, as long as it exceeds sufficiently the cross-section, it is valid except for very low values of ε_L/yL that correspond to a very low premature elastic stress state, which usually are not of interest. In other words, a very large L would not affect the solution; it only makes the solution more general as far as low value of ε_L/yL is concerned. If L is set equal to the depth of the beam, the formulation is valid for first yield and beyond, i.e., elastoplastic and hardening, but invalid prior to that. It must be noted that functions f_i in Eq. (6) must be derived from the origin shown in Fig. 6. Having determined b_n, the FS stress distribution, σ_{FS}, can thus be obtained in terms of *dep* as:

$$\sigma_{FS} = \sum_1^n b_n \sin\left(\frac{n\pi y}{D}\right). \tag{7}$$

Moment capacity formulation for single member

The general expression for moment capacity of a beam can be given as:

$$M = \int_A \sigma(y) y dA. \tag{8}$$

Despite the availability of the general expression of Eq. (8), current practice uses several capacity expressions to cover different stress stages due to the piecewise nature

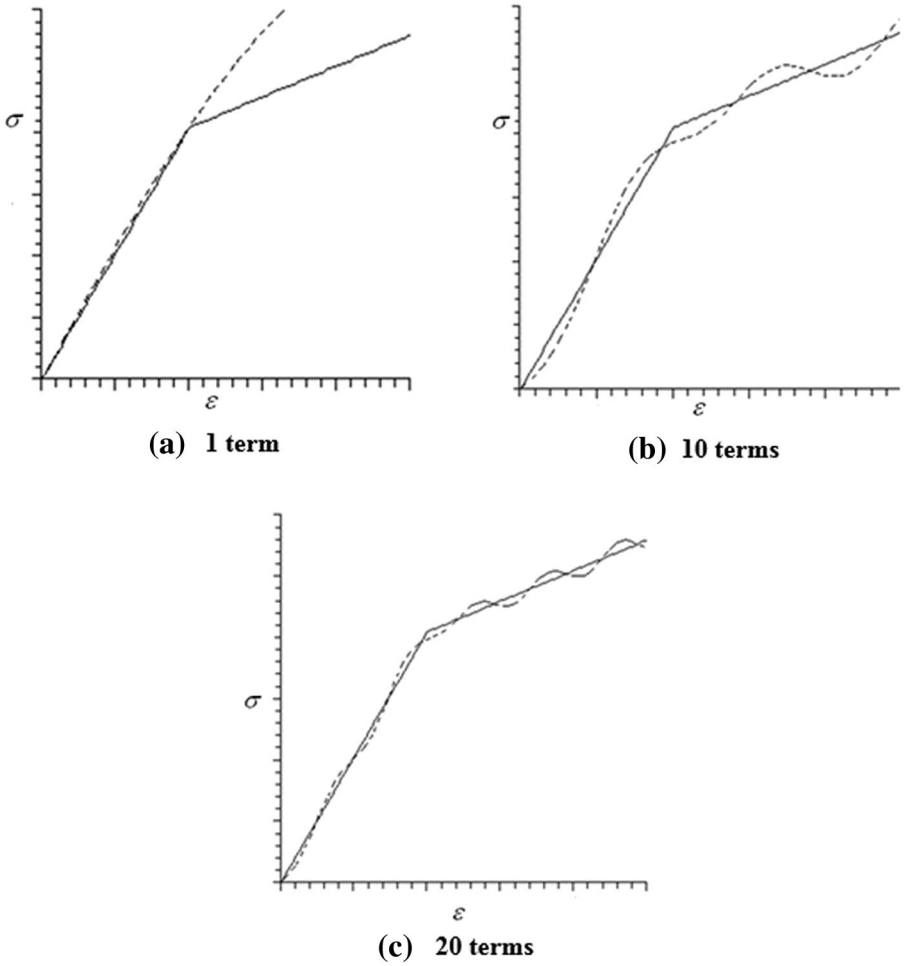

Fig. 3 Representation of typical stress–strain hardening curve by various numbers of FS terms

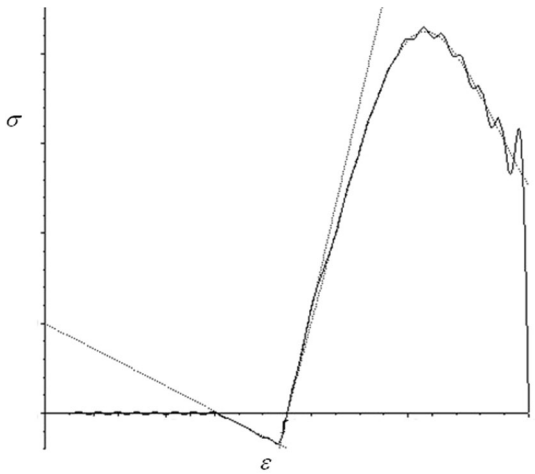

Fig. 4 FS representation of typical concrete material model

of the stress state, i.e., elastic, elastoplastic, plastic. By having a single-rule function represented by the FS, generality of Eq. (8) holds regardless of the stress state. This is the major advantage of the present approach. Inserting Eq. (7) into Eq. (8) will finally give the general moment expression, as follows:

$$M = \int_A \left(\sum_1^n b_n \sin\left(\frac{n\pi y}{D}\right) \right) y \mathrm{d}A. \tag{9}$$

Determination of dep (explicit approach) The unsolved σ_{FS} of Eq. (7) contains *dep* as the unknown variable and, when integrated throughout the area, gives the distribution of the stress resultant, R_{FS} as:

$$R_{FS} = \int_A \sum_1^n b_n \sin\left(\frac{n\pi y}{D}\right) \mathrm{d}A = R_{FS}(dep). \tag{10}$$

To note, Eq. (10) expresses R_{FS} in terms of the unknown, *dep* hence $R_{FS}(dep)$. By setting Eq. (10) to zero, which ensures the satisfaction of the longitudinal equilibrium, *dep* can be solved. The solution of Eq. (10) is best conducted with the aid of commercial programming software, i.e., Matlab (1992) or Maple (2005), using the default command 'solve'.

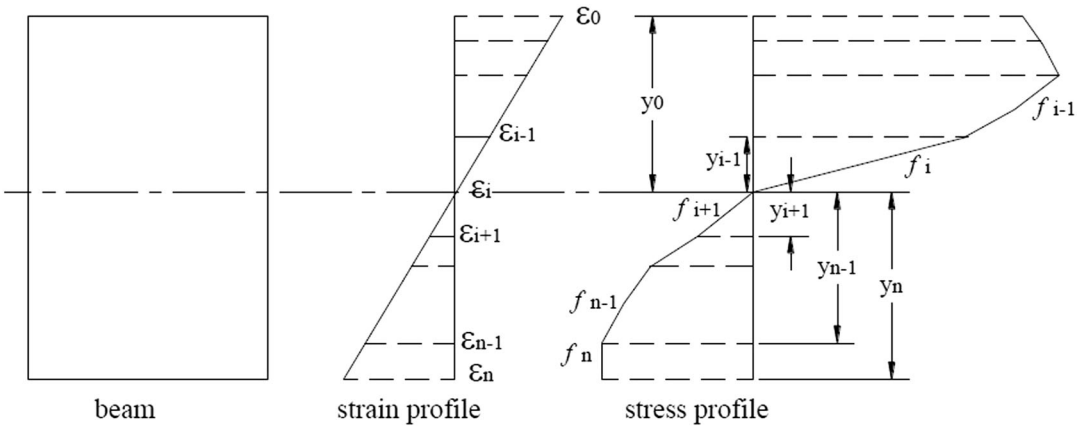

Fig. 5 Piecewise distribution of the strain and the stress

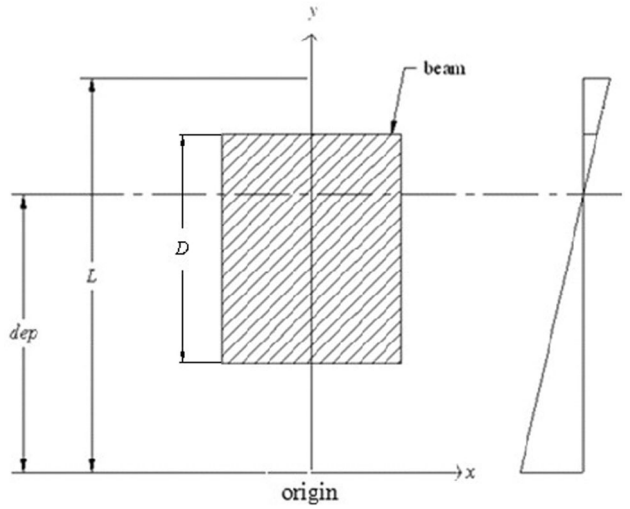

Fig. 6 FS range (or period), L of the cross-section

Determination of dep (graphical approach) As an alternative, a graphical approach can be used to determine the location of *dep*. This is possible because the unsolved R_{FS} is given in terms of *dep*. Varying the value of *dep* throughout the depth of the beam varies the value of R_{FS}; the correct value of *dep* is obtained when R_{FS} intercepts the abscissa. This approach is preferred over the explicit approach as it is much quicker for the commercial software to plot the graph than to solve Eq. (10) explicitly. In Maple, this can be done using the 'plot' command. This approach will be demonstrated in Example 1. Since the preference for the graphical approach over the explicit approach is due to the limitation of current micro-processor capabilities, it should not be seen as resort to an iterative process. With suitable enhancement of computer technology, such a preference is likely to be reversed in the very near future.

Moment capacity for composite member

The preceding formulation is limited to a cross-section composed of a single material. For composite beams, the flexural stress distribution in each material, i.e., steel, concrete, must be represented by FS. At present, the formulation is derived for composite beams with full shear connection. The FS coefficient $b_{n,m}$ of material m can be given in terms of *dep* as:

$$b_{n,m} = \frac{2}{L}\left[\cdots + \int_{dep+y_{i-1},m}^{dep+y_{i,m}} f_{i,m}\sin\left(\frac{n\pi y}{L}\right)\mathrm{d}y + \cdots\right], \tag{11}$$

where subscript m is assigned according to the type of material, i.e., steel, concrete. Having determined $b_{n,m}$, the FS stress distribution, $\sigma_{\mathrm{FS},m}$ can be obtained in terms of *dep* as:

$$\sigma_{\mathrm{FS},m} = \sum_{1}^{n} b_{n,m}\sin\left(\frac{n\pi y}{L}\right) \tag{12}$$

The moment capacity of the beam is thus obtained as:

$$M = \sum_{m=1}\int_{A_m}\left(\sum_{1}^{n} b_{n,m}\sin\left(\frac{n\pi y}{L}\right)\right)y\mathrm{d}A_m + \sum R_{\mathrm{bar}}h_{\mathrm{b}}, \tag{13}$$

where R_{bar} and h_{b} are the rebar resultants and their locations measured from the origin of the FS.

Determination of dep The unsolved $\sigma_{\mathrm{FS},m}$ of Eq. (12) contains *dep* as the unknown and, when integrated throughout the area, gives the distribution of the stress resultant, R_{FS} as:

$$R_{\mathrm{FS}} = \sum_{m=1}\int_{A_m}\sum_{1}^{n} b_{n,m}\sin\left(\frac{n\pi y}{L}\right)\mathrm{d}A_m + R_{\mathrm{FS,bar}}. \tag{14}$$

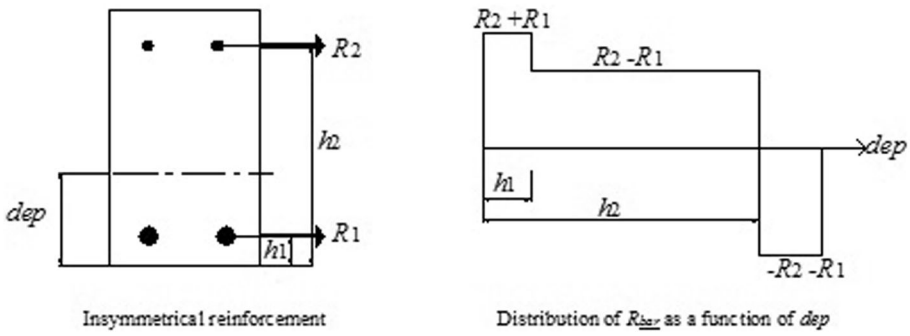

Fig. 7 Piecewise functions of the rebar

By setting Eq. (14) to zero, which ensures longitudinal equilibrium, *dep* can then be solved. The $R_{\mathrm{FS,bar}}$ term is included to incorporate the effect of the rebar when determining the location of the NA. It is a distribution represented by FS, explained as follows.

Consider a beam cross-section as shown in Fig. 7 having unsymmetrically placed rebar, i.e., $R_1 > R_2$. The variation of the total resultant of the rebar as *dep* varies is shown where positive resultants are taken as compressive. This variation can be expressed as a piecewise function as follows:

$$R_{\mathrm{bar}} = \begin{cases} -R_1 - R_2 & \text{if} \quad h_2 \le dep \le L \\ -R_1 + R_2 & \text{if} \quad h_1 \le dep \le h_2 \\ R_1 + R_2 & \text{if} \quad 0 \le dep \le h_1. \end{cases} \tag{15}$$

Having established the piecewise functions, the FS distribution of the rebar resultant can be derived as previously described. For various rebar levels, all that is needed is the extension of the above piecewise functions to cover all ranges. To note, for symmetrical arrangements, i.e., $R_1 = R_2$, the rebars do not affect the location of the NA since they balance each other in the longitudinal equilibrium determination. The quantitative treatment of R_{bar} is demonstrated in Example 2. Similar to the preceding procedure, the *dep* can be obtained either explicitly or graphically.

Worked examples

Worked examples are presented to both validate and demonstrate the application of the formulation.

Example 1: validation of the formulation

This example is intended to validate the formulation by comparing the results with those obtained from the exact method and the simplified stress block method. In the exact method, the result is obtained by direct integration of the piecewise flexural stress distribution of the beam. Consider the complex beam cross-section shown in Fig. 8. The elastic-perfectly-plastic (EPP) steel material curve is assumed. Since the beam is symmetrical about the minor axis, only half the beam is considered. This analysis incorporates the Mohd Yassin and Nethercot (2007) approach. Such incorporation makes the present formulation not only general in terms of stress states but also in terms of composite beam cross-sectional configurations. The material properties of the beam are given in Table 1.

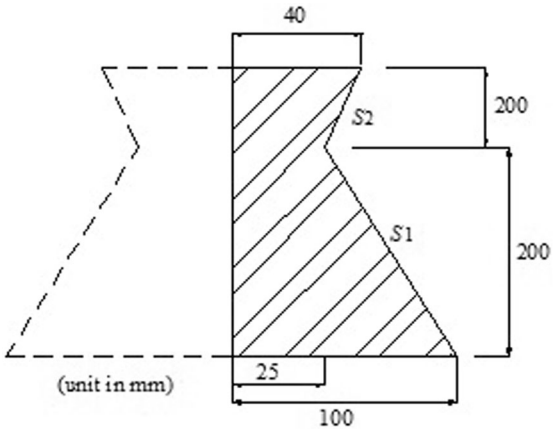

Fig. 8 A complex beam's cross-section

For ease of presentation, the function matrix, FE, the activeness matrix, ACTIVE and the local and the global height vectors, YN and ZN, as required by the approach are given directly herein. For detailed formulations, interested readers are referred to Mohd Yassin and Nethercot (2007).

$$\mathrm{FE} = \begin{bmatrix} 0 & 0 & 1000 - 375y \\ 0 & 0 & 0.075y + 10 \end{bmatrix}, \ \mathrm{ACTIVE} = \begin{bmatrix} 1 & 0 & 0 \\ 1 & 0 & 0 \end{bmatrix}, \ \mathrm{YN} = \begin{bmatrix} 200 \\ 200 \end{bmatrix}, \ \mathrm{ZN} = \begin{bmatrix} 0 \\ 200 \end{bmatrix}.$$

To note, FE must be derived by taking the bottom of the concrete as the origin. Once these matrices are determined, the resultant throughout the depth of the beam, R_{FS}, is thus given as:

Table 1 Material properties of beam for Example 1

Yield stress, $\sigma_y = 280$ N/mm^2	Modulus of elasticity, $E = 2E5$ N/mm^2
Maximum compressive strain, $\varepsilon_L = 0.0022$	Yield strain, $\varepsilon_2 = -\varepsilon_3 = 0.0014$
Beam depth, $D = 400$ mm	FS period, $L = 500$ mm

$$R_{\mathrm{FS}} = \mathrm{ACTIVE}[1,1]\left(\int_{\mathrm{ZN}[1,1]}^{\mathrm{ZN}[1,1]+\mathrm{YN}[1,1]} (\mathrm{FE}[1,3]-\mathrm{FE}[1,2])\mathrm{FS}dy\right) + \mathrm{ACTIVE}[2,1]\left(\int_{\mathrm{ZN}[2,1]}^{\mathrm{ZN}[2,1]+\mathrm{YN}[2,1]} (\mathrm{FE}[2,3]-\mathrm{FE}[2,2])\mathrm{FS}dy\right).$$

The beam is analyzed for its plastic moment capacity condition; therefore, $\varepsilon_0 = 0.1$ is specified. The value of *dep* is obtained graphically by plotting R_{FS} throughout the depth of the beam, as shown in Fig. 9 for various numbers of FS terms *N*, i.e., 50, 100, 150, 200 and 250. Numerical results are given in Table 2.

It can be seen that the FS values approach the 'exact' values as *N* increases. The close agreement between the 'exact' and the rectangular stress block method values justifies the assumption of the full yielding of the steel section. For the moment capacities, calculations are made for four different values of *dep*, where for each value, various *N* values are specified. Figure 10a shows the plot of the moment capacities versus number of terms, *N* whilst Fig. 10b shows the plot of the moment capacities versus various values of the *dep*. Comparison between the two plots provides very important observations. It can be seen that:

1. except for $N = 10$, the gradients of the curves in Fig. 10a are much more gentle than those in Fig. 10b
2. the band of the curves in Fig. 10a is narrower than that in Fig. 10b.

Based on these observations, it can be concluded that the calculation of the moment capacities is more sensitive to the number of terms, *N* in the calculations of the capacity itself as compared to the variations of the *dep*. In other words, while it may be necessary to use a large value for *N* for the moment integration, fewer terms may be sufficient for the determination of *dep*. For example, using *dep* = 124.5564 mm, obtained from $N = 50$, moment capacity of 5.3941×10^8 Nmm is calculated, for $N = 250$. This is just 2% different from using $N = 250$ for both *dep* and the capacity calculation, i.e., 5.4186×10^8 N mm. This is very useful since the expression for the location of the NA [Eqs. (10), (14)] contains two variables, *y* and *dep* whilst the expression for moment [Eqs. (9), (13)] contains only variable *y*. For a given *N*, greater computer resources are required to solve the former as compared to the latter. Therefore, this conclusion gives some sort of balance in terms of the demand on computer resources.

Example 2: performance of the composite beams

This example is intended to demonstrate the generality and the application of the formulation where several equivalent composite cross-sections are analyzed in terms of their

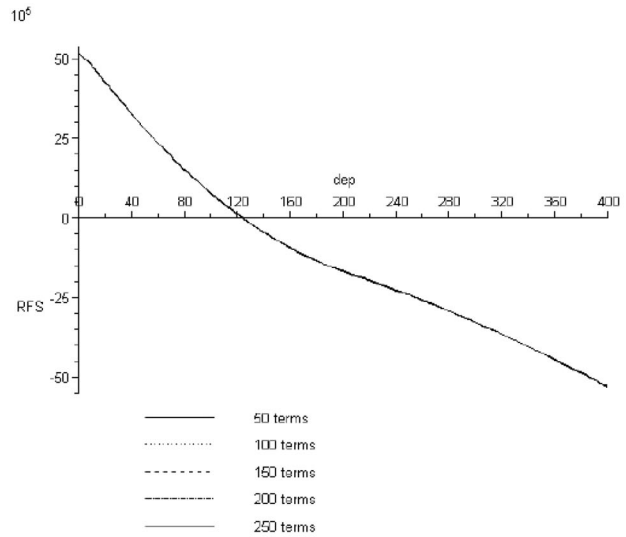

(a) variation of R_{FS} throughout the beam's depth

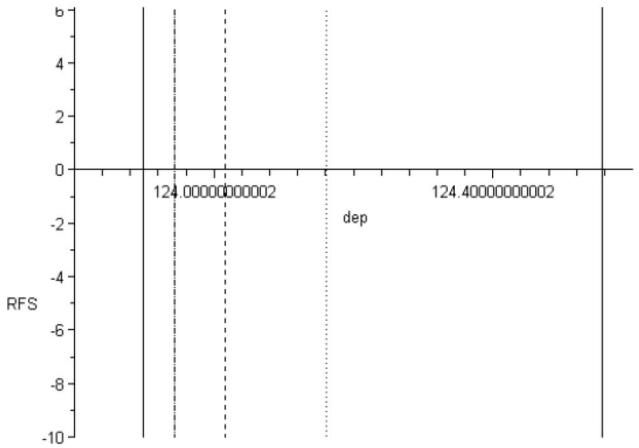

(b) intersection of R_{FS} at the abscissa (magnification of (a))

Fig. 9 Graphical determination of *dep* (unit in mm)

Table 2 Numerical results for Example 1

N	*dep* (mm)			Moment (1×10^8 N mm)					
	Present	Piecewise	Stress block	*dep* = 127.0864	*dep* = 124.5564	*dep* = 124.0149	*dep* = 123.8984	Piecewise	Stress block
10	127.0864	123.700	123.6826	5.0044	5.1054	5.1268	5.1314	5.4440	5.4441
50	124.5564			5.2422	5.3367	5.3570	5.3614		
100	124.1612			5.2785	5.3726	5.3928	5.3971		
150	124.0149			5.2905	5.3845	5.4047	5.4090		
200	123.9423			5.2965	5.3905	5.4107	5.4150		
250	123.8984			5.3001	5.3941	5.4143	5.4186		

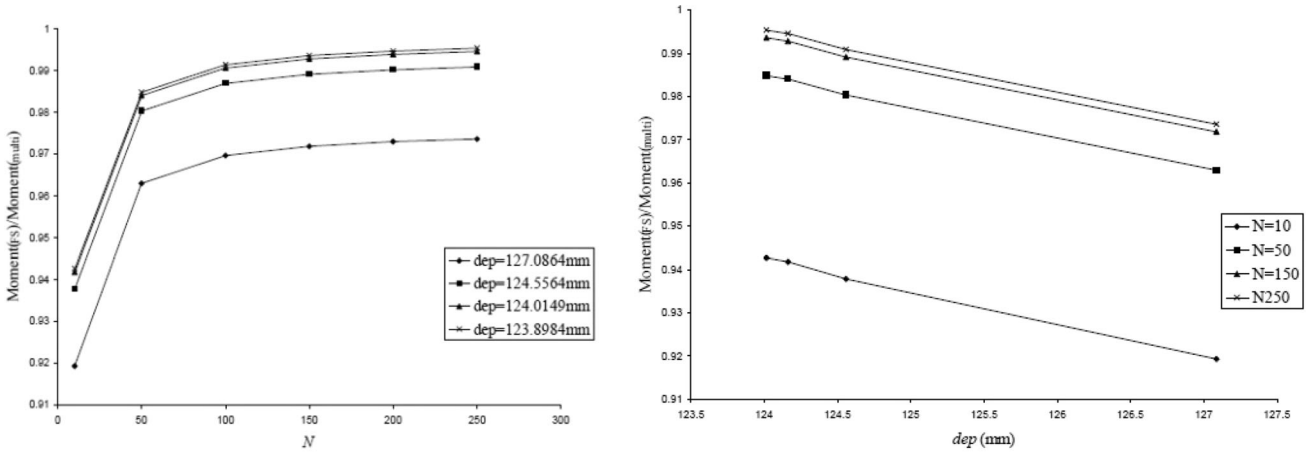

(a) moment versus *N* **(b)** moment versus *dep*

Fig. 10 Sensitivity to the number of FS terms, *N*

moment capacities, as shown in Fig. 11. These beams are equivalent in terms of the amount of steel and the overall depth. Material properties of the beams are given in Table 3. The moment capacity is based on the limiting strain of 0.0035, representing the attainment of the concrete crushing. Herein, elastic–perfectly plastic (EPP) models are used for both the steel and the concrete. All beams have symmetrical rebar arrangements about the major axis (moment contributed by the rebar is 2.61×10^7 N mm), except for the conventional composite beam. The FS representation of the rebar resultants for the conventional composite beam is shown in Fig. 12. This is the quantitative distribution of Fig. 7.

The results of the analysis are given in Table 4. Of the newer forms of beam, Gohnert's beam has the highest moment capacity. The main reason for this is due to the very low placement near the bottom of the beam; the whole steel section has fully yielded in tension. The partial yielding of the steel sections has been captured graphically in Fig. 13. As can be seen, the profiled composite beam has the greatest unyielded portion of steel as shown in Fig. 13a, resulting in the lowest moment capacity. Based on Table 4, the unyielded portion of the profiled composite beam amounted to a depth of 107.32 mm. The PCFC beam, although it has a moderate moment capacity, contains 23.5% less concrete as compared to the other beams and thus is the lightest. For this particular configuration, the elastic neutral axis depth of the PCFC is calculated as 24.88 mm. But, if the location of the steel section in the PCFC is lowered, greater moment capacity can be expected. The partial yielding of the contemporary beams highlights the acceptance of concrete crushing as one type of premature failure. As compared to the conventional composite arrangement, which has been shown in Fig. 13b to have full yielding of the steel section, the possibility of partial yielding of the steel due to the concrete crushing for the contemporary beam is based on the fact that the concrete and the steel are placed at the same levels, leading to deeper location of the NA. Since they are assumed to have the same strain profile, such a configuration produces relatively larger strains at the concrete extreme fiber as compared to a shallower concrete arrangement, i.e.,

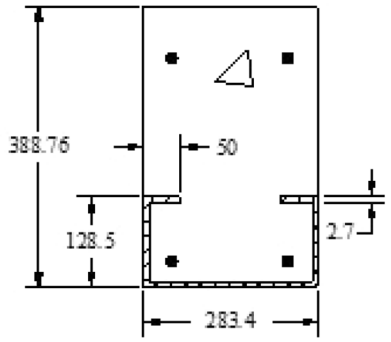

(a) Gohnert and Komakec (2005)[4]

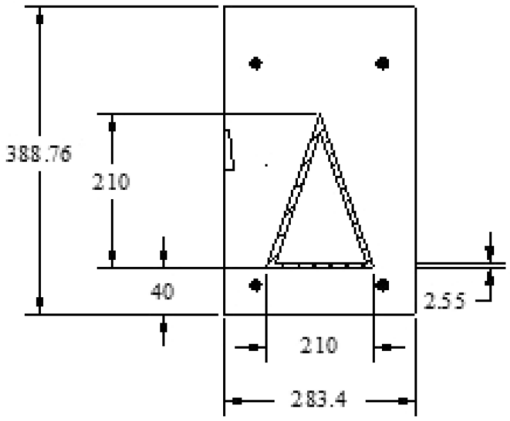

(b) PCFC beam (Yassin and Nethercot, 2007[8])

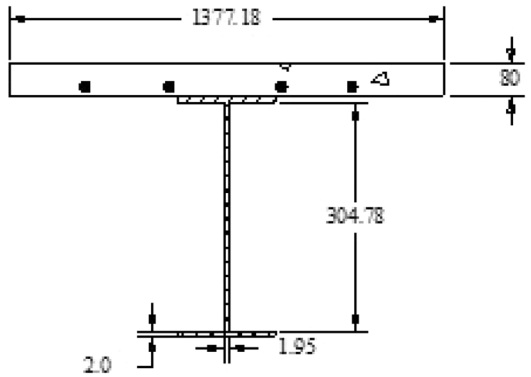

(c) Conventional composite beam

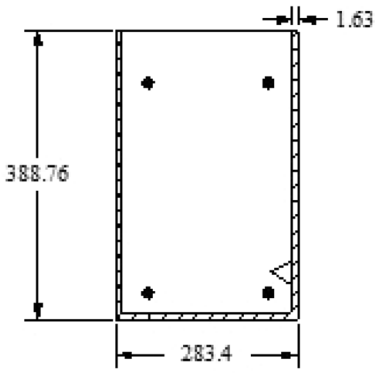

(d) Profiled composite beam (Uy and Bradford, 1994[19])

Fig. 11 Equivalent composite beams in terms of amount of steel and total depth (dimensions in mm)

Table 3 Material properties for Example 2

Properties	Concrete	Steel sheeting	Reinforcement bar
Modulus of elasticity E (N/mm^2)	33,100	205,000	200,000
Cylinder compressive strength, 0.85 f_c (N/mm^2)	36.89	–	–
Yield strength, p_y or 0.87 f_y (N/mm^2)	–	552	378.45

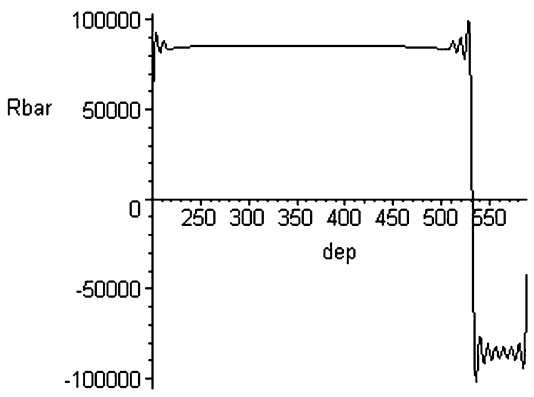

Fig. 12 FS representation of the distribution of the rebar resultants (units in N and mm)

concrete slab in the conventional beam. However, despite the full yielding of the steel section in the conventional composite beam, its moment capacity is relatively low. Further investigation has revealed that this low capacity is due to the partial crushing of the concrete. Figure 14 shows the state of stress in the concrete element for all beams. Except for Fig. 14b, which is the stress distribution based on the rigid-plastic model, the other distributions are based on the EPP model. As can be seen, due to the use of the EPP model a large elastic region (as compared to the crushing region) exists in the conventional composite beam, whilst for other beams, a substantial crushing region

Table 4 Performance of the beams

Beam	*dep* (mm)	Elastic depth of steel (mm)	Moment (1×10^8 Nmm)
Profiled	519.011	107.32	1.8822
Conventional	563.766	0	1.8422
PCFC	497.716	24.88	1.8938
Gohnert and Komakec (2005)	497.271	0	2.409

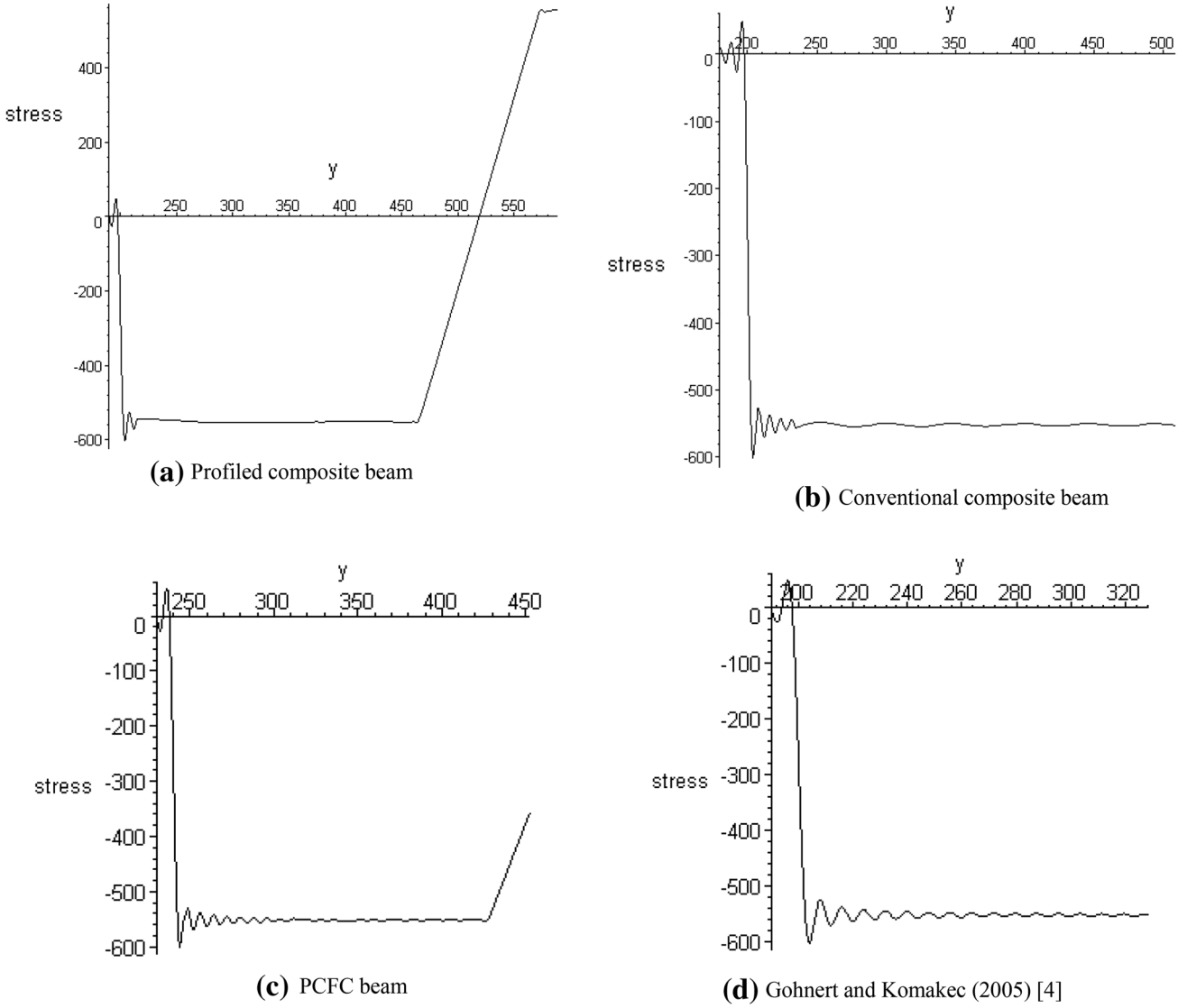

Fig. 13 Yielding of the steel sections (units in N and mm)

can be seen. Such a difference is inferred as being due to the higher location of the NA in the conventional composite beam, which causes the EPP formulation to yield such a distribution. Rerunning the analysis for the conventional composite beam, but this time using the Rigid-plastic model (Fig. 14b), a much higher capacity is obtained (2.9828×10^8 N mm). This demonstrates the sensitivity to material models in the analysis.

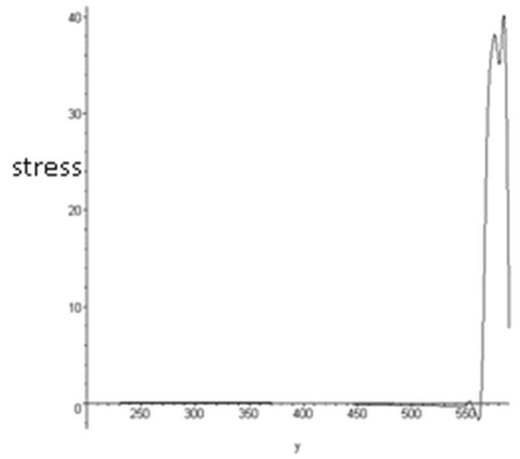

(a) Conventional (EPP)

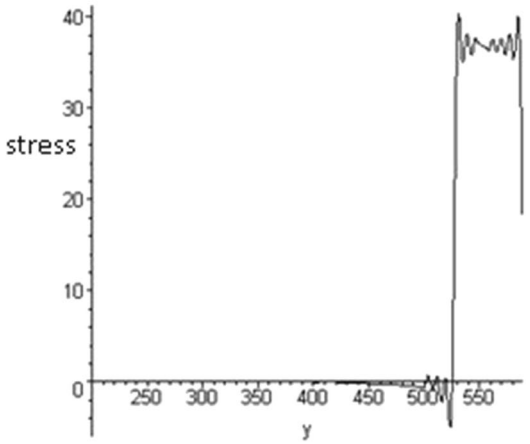

(b) Conventional (Rigid-plastic)

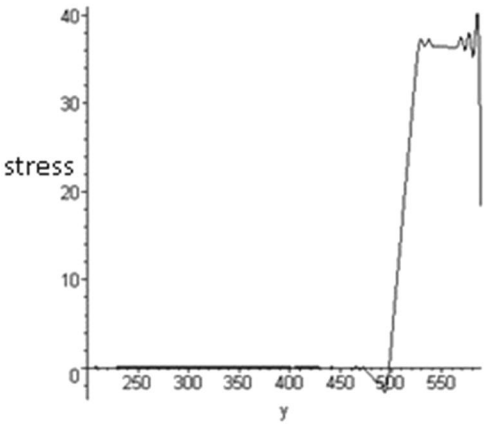

(c) PCFC beam

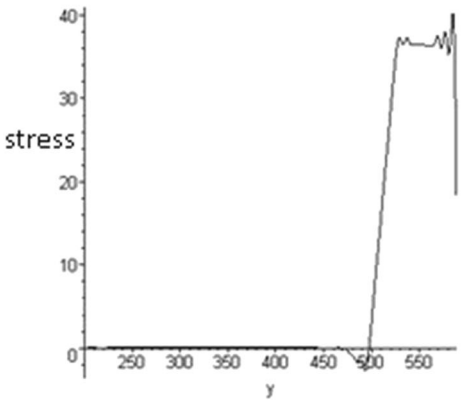

(d) Gohnert and Komakec (2005)

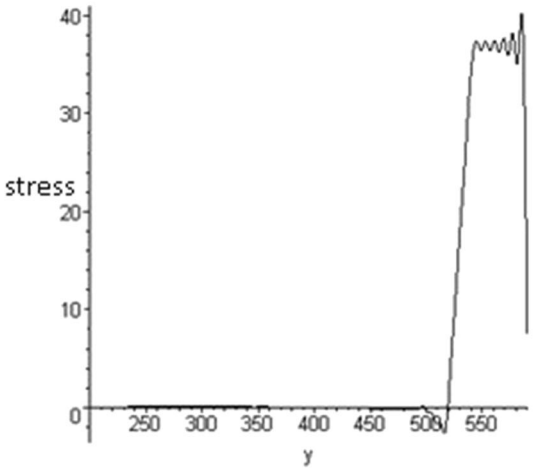

(e) Profiled composite beam

Fig. 14 Partial crushing of concrete (units in N and mm)

Conclusions

A non-iterative procedure for the determination of the moment capacity has been formulated for composite beams. Such a formulation is possible because Fourier series have been utilized to represent the piecewise distributions of the flexural stress as a single-rule function. This allows direct integration of the stress distribution throughout the depth of the beam and, hence, the direct determination of the location of the neutral axis (without the need for iteration). Also, it makes the general moment capacity expression applicable to all stress states. Numerical examples were given which validated the formulation and demonstrated its application. It was shown that, when incorporated into the procedure previously proposed by the authors, the formulation is general for any composite cross-section. It was also shown that the formulation is able to provide detailed information on the stress development within the beam cross-section, i.e., state of yielding and crushing, which are very valuable in better informing the design of the structure.

Acknowledgements The first author would like to thank his sponsors, Public Service Department of Malaysia and Universiti Teknologi Malaysia for their financial support in his PhD undertaking at Imperial College London.

References

Adekola AO (1968) Partial interaction between elastically connected elements of a composite beam. Int J Solids Struct 4:1125–1135

Ayoub A, Filippou FC (2000) Mixed formulation of nonlinear steel-concrete composite beam element. J Struct Eng 124(10): 1148–1158

Carreira DJ, Chu KH (1985) Stress-strain relationship for plain concrete in compression. ACI Struct J 82(11):797–804

Dall'Asta A, Zona A (2002) Non-linear analysis of composite beams by a displacement approach. Comput Struct 80:2217–2228

Gohnert M, Komakec MJ (2005) Steel channel and hollow block floor slabs. Struct Eng 17:30–34

Lodygowski T, Szumigala M (1992) Engineering models for numerical analysis of composite bending members. Mech Struct Mach 20(3):363–380

Maple10, (c) Maplesoft, a division of Waterloo Maple Inc. (2005)

Matlab7, Version 7.0.0 19920 9 (R14) (2004) Copyright The MathWorks, Inc

Mohd Yassin AY, Nethercot DA (2007) Cross-sectional properties of complex composite beams. Eng Struct 29(20):195–212

Newmark NM, Siess CP, Viest IM (1951) Tests and analysis of composite beams with incomplete interaction. Proc Soc Exper Stress Anal 9:75–92

Oehlers DJ, Wright HD, Burnet MJ (1994) Flexural strength of profiled composite beams. J Struct Eng ASCE 120(2):378–390

Ranzi G, Gara F, Leoni G, Bradford MA (2006) Analysis of composite beams with partial shear interaction using available modeling techniques: a comparative study. Comput Struct 84:930–941

Roberts TM, Haji-Kazemi H (1989) Theoretical study of the behaviour of reinforced concrete beams strengthened by externally bonded steel plate. Proc Inst Civil Eng Part 2 87(1):39–55

Robinson H, Naraine KS (1998) Slip and uplift effects in composite beams. In: Buckner CD, Viest IM (eds) Composite construction in steel and concrete. ASCE, New York, pp 487–497

Smith ST, Teng JG (2001) Interfacial stresses in plated beams. Eng Struct 23:857–871

Sousa JBM Jr, Muniz CFDG (2007) Analytical integration of cross-section properties for numerical analysis of reinforced concrete, steel and composite frames". Eng Struct 29:618–625

Taljsten B (1997) Strengthening of beams by plate bonding. J Mater Civil Eng ASCE 9(4):206–212

Teng JG, Chen JF, Smith ST, Lam L (2001) FRP strengthened RC structures. Wiley, Chichester, UK

Uy B, Bradford MA (1994) Inelastic local buckling behaviour of thin steel plates in profiled composite beams. Struct Eng 72(16):259–267

Uy B, Bradford MA (1995a) Local buckling of thin steel plates in composite construction: experimental and theoretical study. Proc Inst Civil Eng Struct Build 110:426–440

Uy B, Bradford MA (1995b) Ductility of profiled composite beams. Part 2: analytical study. J Struct Eng ASCE 121(5):883–889

Uy B, Bradford MA (1996) Elastic local buckling of steel plates in composite steel-concrete members. Eng Struct 18(3):193–200

Wright HD (1993) Buckling of plates in contact with a rigid medium. Struct Eng 71(12):209–215

Wright HD (1995) Local stability of filled and encased steel sections. J Struct Eng ASCE 121(10):1382–1388